Geophysical Prospecting EAGE EUROPEAN ASSOCIATION OF GEOSCIENTISTS & ENGINEERS

Geophysical Prospecting, 2013, **61** (**Suppl. 1**), 391–408 doi: 10.1111/j.1365-2478.2013.01125.x

A comparison of shot-encoding schemes for wave-equation migration

Jeff Godwin* and Paul Sava

Center for Wave Phenomena, Colorado School of Mines

Received November 2011, revision accepted May 2012

ABSTRACT

In the last decade the seismic imaging industry has begun collecting data volumes with a substantial amount of data redundancy through new acquisition geometries including: wide-azimuth, rich-azimuth and full-azimuth geometries. The increased redundancy significantly improves image quality in areas with complex geology, but requires considerably greater computational power to construct an image because of the additional data and the need to use advanced imaging algorithms. One way to reduce the computational cost of processing such datasets is to blend shot-records, using shot-encoding, together prior to imaging which reduces the number of migrations necessary for imaging. The downside to doing so is that blending introduces strong, non-physical, cross-talk noise into the final image. By carefully choosing the shot-encoding scheme, we can reduce the additional noise inserted into the image and maximally reduce the number of migrations necessary. We describe a theory of blended imaging that explains all shot-encoding schemes, and use the theory to design a new class of encodings that use amplitude weights instead of phase-shifts or time-delays. We are able to use amplitude encoding to produce blended images of the same quality as previous encoding schemes at a similiar computational cost. Furthermore, we compare the results of amplitude encoding with the results from well-known shot-encoding schemes from previous work including: plane-wave migration, random-time delay, modulated-shot migration, and decimated shot-record migration. In our comparison, we find that plane-wave migration is in many ways an optimal shot-encoding scheme. However, we find that plane-wave migration produces results that are comparable to decimated shot-record migration when the total cost of imaging is taken into account, thereby calling into question the utility of shot-encoding in general. Overall, this work questions the potential for shot-encoding in standard (shot-record) seismic imaging because blended imaging does not appear to sufficiently reduce the cost of imaging given the quality of the blended image compared to decimated shot-record migration.

.

INTRODUCTION

Today's seismic exploration challenges include imaging areas with complex geology, such as salt domes and overthrust regions. The major issues for imaging areas with complex geology are poor data quality and lack of seismic illumination due to the severe deformation of the seismic wavefield. One approach to resolve these issues is to obtain large amounts of redundant information from various acquisition directions via wide-azimuth or full-azimuth seismic surveys (Michell *et al.* 2006; Shoshitaishvili *et al.* 2006; Howard 2007; Kapoor *et al.*

* Email: godwin.jeffrey@gmail.com

2007; Ting and Zhao 2009). However, wide-azimuth surveys require significantly more time to acquire and even greater amounts of time to process due to the large amounts of data. Subsequently, the cost of acquiring and processing a wide-azimuth survey is significantly more expensive than the cost of a conventional survey. Additionally, the cost of imaging in complex geology is much greater because advanced imaging algorithms such as reverse-time migration must be used to better honor the kinematics of complex wavefields. Therefore, both the financial and computational cost of today's large surveys is increasing at a rapid pace, but recent technological advances may allow us to reduce these costs by using better processing technologies and faster computers for imaging.

One such technology is acquisition using simultaneous or delayed sources (Womack 1990; Hampson, Stefani and Herkenhoff 2008; Berkhout, Blacquiere and Verschuur 2008; Beasley 2008; Blacquiere, Berkhout and Verschuur 2009). As the name implies, simultaneous sources are triggered at the same time but at different spatial locations. By acquiring multiple sources in a shot-gather, a full-survey may be acquired in much less time than what is currently required. The downside to simultaneous source acquisition is that it creates additional noise in the final seismic image. Past research has circumvented the additional noise by de-blending the simultaneous source shot-gathers to create separate shot-gathers, as would be collected in a conventional survey, for each source prior to imaging (Spitz, Hampson and Pica 2008; Moore *et al.* 2008; Hampson *et al.* 2008; Akerberg *et al.* 2008; Kim *et al.* 2009; Huo, Luo and Kelamis 2009). The separated shot-gathers are imaged using conventional shot-record migration (SRM) to produce the final image. The drawback to separating the shots is two-fold:

- First, the sources must be separable, which typically implies that they are relatively isolated from one another in space and/or time. This constraint limits the maximum amount of shots that can be used at once during acquisition.
- Second, the imaging process is not sped up by separating the shots because each separated shot must be imaged separately, as in SRM.

A related idea, that aims to reduce the cost of imaging large datasets is to use multiple sources at once during imaging, which emulates simultaneous source acquisition. This process, known as blended imaging, combines multiple shot-gathers together prior to migration, which reduces the number of migrations that are needed to produce a final image (Morton 1999; Liu 1999; Romero *et al.* 2000; Soubaras 2006; Zhang, Sun and Gray 2007; Perrone and Sava 2009; Berkhout, Verschuur and Blacquiere 2009). Certain forms of blended imaging, most notably plane-wave migration, are used in industry today, but many forms of blending (e.g. random phase) are not used today because they introduce a significant amount of noise to the image, known as crosstalk noise. However, the presence of the noise may be justified if the cost advantage over conventional shot-record migration is sufficiently high.

Previous attempts to remove the crosstalk noise from the shot-encoded images have focused on phase-shifting the shot-records to shift the wavefields out of phase with one another as in plane-wave migration Tieman (1997), and random phase encoding Morton (1999). Recently, a variety of phase-encoding schemes have been developed including: plane-wave (Temme 1984; Tieman 1997; Stork 1999; Liu 1999; Duquet 1999; Stoffa *et al.* 2006; Zhang *et al.* 2005; Liu *et al.* 2006; Shan and Biondi 2008), random (Romero *et al.* 2000), harmonic (Zhang *et al.* 2007), plane-wave with dithering (Perrone and Sava 2009), and frequency dependent, sign-opposite (Sun 1999). It is important to note that many of these schemes choose to use linear phase-shifts as a function of frequency, and are therefore time-delay encodings. Of these encoding schemes, plane-wave is the most widely used. Another recently developed encoding scheme is to use frequency independent phase-shifts in a modulated migration scheme (Soubaras 2006).

Regardless of the shot-encoding scheme chosen, the most powerful method for attenuating crosstalk noise is to simply stack the images over many blended experiments (or realizations) that have different crosstalk characteristics because the desired image stacks together, while the incoherent crosstalk noise stacks out (Romero *et al.* 2000). However, simple stacking is not sufficient to completely remove most of the crosstalk for many shot-encoding schemes at a suitable cost advantage over shot-record migration because crosstalk noise is not completely incoherent from one blended experiment to another (i.e. crosstalk noise stacks together) (Romero *et al.* 2000). Thus, it is crucial to select encoding schemes that minimize the crosstalk noise during the imaging process. Subsequently, the two most important unresolved questions regarding blended imaging are: Does an optimal shot-encoding scheme exist that produces the best possible image at the lowest possible computational cost? If not, which of the already known shot-encoding schemes should be used?

The main goal of our work is to compare the suitability of various shot-encoding schemes for reducing the computational cost of imaging. By doing so, we aim to demonstrate which shot-encoding schemes produce the best image at the lowest possible cost. Towards this objective, we restate a theory of blended imaging, that while not novel, reframes the

process of shot-encoding in terms of matrix operations which helps develop an intuitive understanding of shot-encoding. Using the theory that we outline, we develop a new class of shot-encoding schemes using amplitude weights only, which are comparable to existing shot-encoding schemes in terms of cost and image quality. We compare the outcomes of: amplitude encoding, plane-wave migration, modulated-shot migration, random time-delay encoding, and decimated shot-record migration in imaging the Sigsbee2A salt dataset. Overall, we find that plane-wave migration is the best shot-encoding scheme presented. However, a theoretical computational cost analysis of shot-encoding, that compares both image quality and cost, demonstrates that decimated shot-record migration typically produces images comparable in quality to shot-encoding at the same total computational effort for the given scenario. We conclude by discussing the scenarios under which one should prefer shot-encoding to decimation and vice-versa, although for many real-world datasets decimation appears to be preferred.

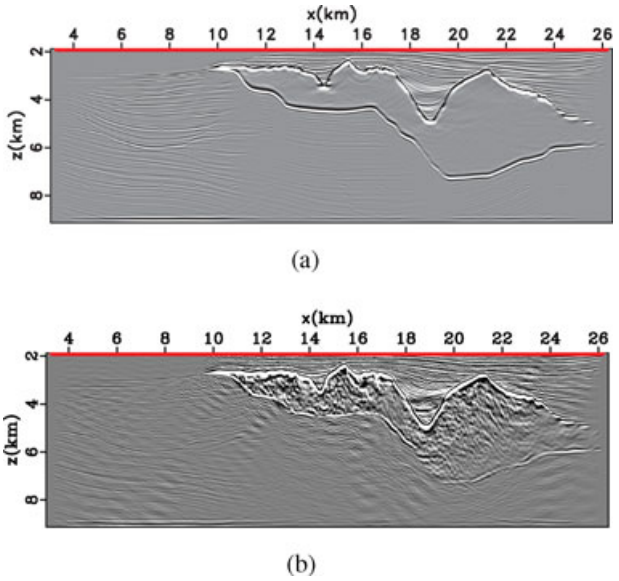

Figure 1 An example of how crosstalk contaminates the final stacked image for blended images. The (a) image obtained by conventional shot-record migration, (b) is the image obtained by random time-delay encoding, which introduces crosstalk artifacts that severely degrade the quality of the image.

THEORY

In this section, we develop a theory of shot-encoding beginning with basic principles, continuing through the development of a matrix representation of shot-encoding, and concluding with an analysis of the theoretical cost considerations of blended imaging.

Basic principles of shot-encoding

As previously mentioned, shot-encoding (blending) is a process during which the individually acquired shot-records are linearly combined with one another in order to reduce the number of migrations necessary for imaging. During the blending process, each shot-record is individually weighted (or phase-shifted) and then all the weighted shot-gathers are summed together to form a blended shot-gather prior to migration (Morton 1999; Liu 1999; Romero *et al.* 2000; Soubaras 2006; Zhang *et al.* 2007; Perrone and Sava 2009; Berkhout, Verschuur and Blacquiere 2009). To form a shot-encoding scheme, a series of blended shot-gathers are produced by changing the weights for each shot-record from one blended experiment to another. The way that the weights are changed from experiment to experiment, determines the type of encoding, and the characteristics of that encoding scheme (Liu 1999; Romero *et al.* 2000; Perrone and Sava 2009). After the shot-records are encoded, the source- and receiver-wavefields are reconstructed for the blended experiments exactly as in conventional shot-record migration. To produce an image using the blended wavefields we can apply the conventional cross-correlation imaging condition to the reconstructed wavefields as follows,

$$R_e(\mathbf{x}) = \sum_e \sum_t \left(\sum_i A_e^i W_s^i(\mathbf{x}, t) \right) \left(\sum_j A_e^j W_r^j(\mathbf{x}, t) \right), \qquad (1)$$

where i and j are the shot-record indices, $W_s^i(\mathbf{x}, t)$ is the i^{th} reconstructed source wavefield, $W_r^j(\mathbf{x}, t)$ is the j^{th} reconstructed receiver wavefield, e represents the blended shot-gathers index, A_e^i or A_e^j represents the shot-encoding weight for i^{th} or j^{th} shot-record for the e^{th} blended experiment, t represents time, $\mathbf{x}$ is a vector of locations in space. When $i = j$, equation (1) computes the correlation of wavefields related to a single shot gather. Conversely, when $i \neq j$, equation (1) computes the image for wavefields that are not physically related to one another, which introduces strong, coherent noise into the image that is indistinguishable from the desired image. This strong noise is referred to as crosstalk (Romero *et al.* 2000). As equation (1) shows, the crosstalk terms exist for each blended experiment for each source and every other receiver wavefield which means that there is a significant amount of crosstalk in the final image. Due to the negative impact of crosstalk noise on final image quality, crosstalk noise must be sufficiently attenuated during the imaging procedure.

Matrix representation of imaging

As previously noted by Tieman (1997) and Soubaras (2006) conventional seismic imaging can be described by a series of matrix operations, which can be expanded to include blended source imaging. Additionlly, the matrix representation allows us to determine the overall suitability of a shot-encoding scheme by determining the amount of crosstalk in the migrated image in advance.

To start, we revisit conventional shot-record migration, which is composed of two steps: wavefield reconstruction and the application of an imaging condition, which produces an image R as follows,

$$R(\mathbf{x}) = \sum_t \sum_i W_s^i(\mathbf{x}, t) W_r^i(\mathbf{x}, t). \tag{2}$$

For each shot gather, the source- and receiver-wavefields, W_s^i and W_r^i respectively, are reconstructed separately. Then, the two wavefields are cross-correlated and summed over time or frequency, depending on the domain, to form a partial image. All of the partial images are then stacked together to form the final image. Mathematically, each source and receiver-wavefield can be thought to be an element in a vector that holds all source- or receiver-wavefields respectively,

$$\mathbf{W}_S = \left[W_S^1, W_S^2, \ldots, W_S^i, \ldots, W_S^{N_s} \right], \tag{3}$$

$$\mathbf{W}_R = \left[W_R^1, W_R^2, \ldots, W_R^i, \ldots, W_R^{N_s} \right], \tag{4}$$

where $\mathbf{W}_S$ and $\mathbf{W}_R$ are row vectors, N_s is the number of shot-gathers, composed of the reconstructed wavefields, W_S^i and W_R^i, respectively. The i^{th} elements of both $\mathbf{W}_S$ and $\mathbf{W}_R$ correspond to the same physical shot-gather. Thus, conventional seismic imaging is equivalent to the inner product of the two vectors,

$$R = \mathbf{W}_S \mathbf{W}_R^H, \tag{5}$$

where R is the constructed image, H is the complex-conjugate transpose, and the multiplication of two elements of the matrix is actually the application of the imaging condition between those wavefields. As indicated earlier, the application of the imaging condition implies a summation over either time or frequency depending on which domain we use for wavefield reconstruction. The summation over elements of the vectors implies stacking the partial images together.

The encoding matrix

In order to expand this notation to blended source imaging, we make use of the encoding matrix $\mathbf{E}$ (Tieman 1997; Soubaras 2006). The encoding matrix is $N_s \times N_e$, where N_e is the number of blended experiments and N_s is the number of shots (wavefields) in the survey. Each column in the encoding matrix corresponds to a single blended experiment (realization), while each row acts as a weight for a particular source- or receiver-wavefield. Thus, each column in the encoding matrix weighs all wavefields to determine how to combine them together prior to imaging. To formally define the encoding matrix, we introduce the notation $E_{m,n}$, where the m index corresponds to the row (or shot index) and n corresponds to the column, or blended experiment index. The encoding matrix contains weights which may be fractional, positive or negative, and may even be complex-valued and can be described as follows,

$$\mathbf{E}_{m,n} = A_{m,n} \exp(-j\phi_{m,n}), \tag{6}$$

where A is the amplitude weight for the m^{th} shot-record for the n^{th} blended experiment, $\phi_{m,n}$ is the corresponding phase-shift for that shot-record, and j is $\sqrt{-1}$. Amplitude only encodings are represented in equation (6) by letting $\phi_{m,n} = 0$ for all m and n. Conversely, phase-encodings are obtained when $A_{m,n} = 1$ for all m and n.

Because we generally assume that we can treat frequencies independently from one another, a different encoding matrix may exist for each frequency simultaneously. Thus, the encoding matrix is actually a three-dimensional matrix whose third dimension is frequency, ω, and $\mathbf{E}$ is a function of ω in the most general case (Soubaras 2006). Mathematically, we represent the frequency-dependence of an element in the encoding matrix as:

$$\mathbf{E}_{m,n}(\omega) = A_{m,n}(\omega) \exp(-j\phi_{m,n}(\omega)) \tag{7}$$

where $A_{m,n}(\omega)$ is the amplitude weight for the frequency, ω, and $\phi_{m,n}(\omega)$ is the phase-shift for the same frequency. A special case of frequency dependent phase-encodings are time-delay encodings where $\phi_{m,n}(\omega) = 2\pi\omega\tau_{m,n}$, which causes a linear-shift of phase as a function of frequency. Due to the symmetry of the time and frequency domain, it is also possible to consider time-dependent encodings, where a different encoding is used for each time-step, but it is not clear if there is an advantage to doing so.

For simplicity we only consider the frequency independent case where $\mathbf{E}(\omega) = \mathbf{E}$ for all ω, but the framework that we develop is equally valid for both frequency dependent and

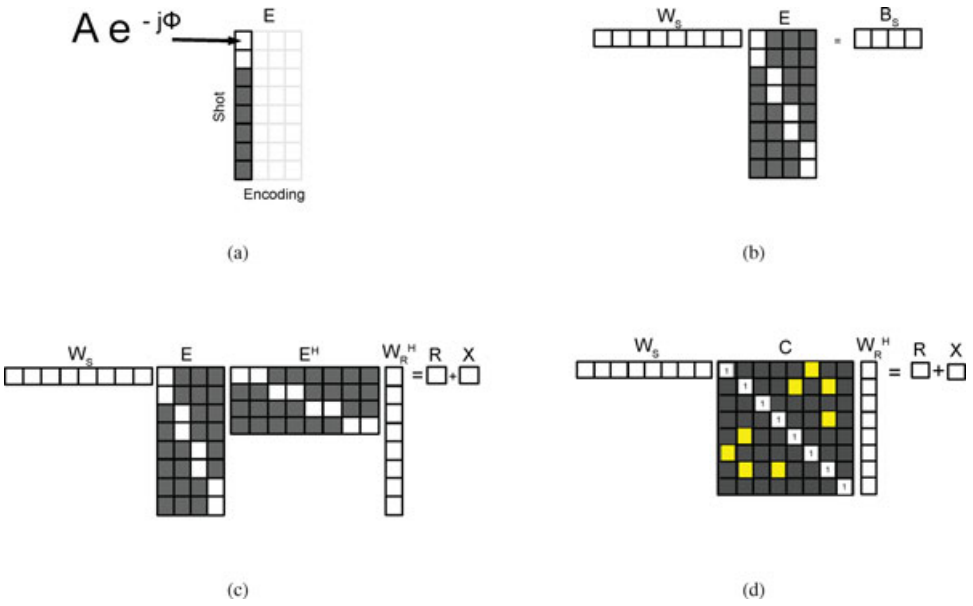

Figure 2 The encoding matrix (a) is composed of weights of the form $A\exp(-j\phi)$ where A is the amplitude weighting term, and ϕ is the phase-shift to be applied. To blend the wavefields, we project the wavefield vector onto the encoding matrix (b) to produce the blended wavefield vector $\mathbf{B}_S$. By performing the necessary substitutions, the entire blended imaging process (c) can be summed up as the product of matrix multiplications. The crosstalk matrix (d) is the product of the encoding matrix with its transpose. In these diagrams, the shot-encoding scheme is a binary (1 or 0) amplitude encoding (i.e. $\phi = 0$) scheme where the white cells indicate one, and the gray cells indicate zero in the encoding and crosstalk matrices.

frequency independent encodings. For reference, Figure 2(b) depicts a sample amplitude-only encoding matrix where the weights are real-valued, binary (1 or 0) whose effect is to select only some wavefields per blended experiment.

Matrix representation of blended imaging

The encoding matrix reduces the effective number of reconstructed wavefields that are used for imaging by projecting the wavefield vector onto the encoding matrix, thereby reducing the dimensionality of the wavefield vector as follows:

$$\mathbf{B} = \mathbf{WE}, \text{ then } \begin{cases} \mathbf{B}_S = \mathbf{W}_S\mathbf{E} \\ \mathbf{B}_R = \mathbf{W}_R\mathbf{E} \end{cases}, \tag{8}$$

where $\mathbf{WE}$ is the projection of the wavefield vector (i.e. $\mathbf{W}_S$ or $\mathbf{W}_R$) onto the encoding matrix $\mathbf{E}$, and $\mathbf{B}$ is the blended wavefield vector for the source- or receiver-wavefields (i.e. $\mathbf{B}_S$ or $\mathbf{B}_R$). Therefore, $\mathbf{B}_S$ is the $1 \times N_e$ row vector of combined source-wavefields and $\mathbf{B}_R$ is an $1 \times N_e$ column vector of combined receiver-wavefields. Because the migration operator is linear, we can perform the combination of the source- and receiver-data, the product of $\mathbf{WE}$, prior to wavefield reconstruction, thus reducing the necessary number of migrations from N_s to N_e. The final blended source image R_e is represented by

$$R_e = \mathbf{B}_S\mathbf{B}_R^H, \tag{9}$$

and is shown in Figure 2(c). By substituting the expressions for $\mathbf{B}_S$ and $\mathbf{B}_R$ from equation (8) into equation (9), we obtain:

$$R_e = \mathbf{W}_S\mathbf{E}\mathbf{E}^H\mathbf{W}_R^H, \tag{10}$$

which is similar to equation (5) and shown in Figure 2(c). We refer to the product $\mathbf{EE}^H$ as the crosstalk matrix $\mathbf{C}$, which is square and has dimensions of $N_s \times N_s$, Figure 2(d). The crosstalk matrix $\mathbf{C}$ is similar to the identity $\mathbf{I}$, but with additional off-diagonal terms as shown in 2(d). This is a convenient description because equation (5) can be rewritten to include the identity matrix $\mathbf{I}$ to represent the pairing of each source wavefield with its corresponding receiver wavefield as:

$$R_e = R + X = \mathbf{W}_S\mathbf{I}\mathbf{W}_R^H + \mathbf{W}_S(\mathbf{C} - \mathbf{I})\mathbf{W}_R^H. \tag{11}$$

Thus, the $\mathbf{C}$ matrix represents the formation of the conventional seismic image (i.e the identity diagonal terms) plus additional terms in the off-diagonals (and potentially deviations from the diagonal identity terms) representing the pairing of wavefields that are not physically related to one another.

Subsequently, the off-diagonal components of the **C** matrix are the crosstalk terms that we generate by using a certain encoding matrix **E** (Tieman 1997; Soubaras 2006).

Designing optimal shot-encoding schemes

By examining equation (11), we find that optimal shot-encoding schemes should have a crosstalk matrix **C** that is as close to the identity matrix **I** as possible in order to minimize the crosstalk in the image R_e, (Tieman 1997; Soubaras 2006). Consequently, the process of choosing a shot-encoding scheme becomes one of finding an encoding matrix **E** such that $\mathbf{E}\mathbf{E}^H$ has the fewest off-diagonal components, or $\mathbf{E}\mathbf{E}^H \approx \mathbf{I}$. If an encoding exists such that $\mathbf{E}\mathbf{E}^H = \mathbf{I}$, then we can produce the same image as shot-record migration, at a cost proportional to the number of blended source experiments N_e, instead of N_s (Soubaras 2006).

One possible set of encoding matrices are orthonormal bases. For reference, a matrix **Q** is defined to be an orthonormal basis if $\mathbf{Q}^H\mathbf{Q} = \mathbf{I}$ and $\mathbf{Q}\mathbf{Q}^H = \mathbf{I}$, which implies that the row and column vectors are orthogonal to one another, and that the norm of each vector is one. Thus, we reconstruct the identity matrix **I** from $\mathbf{E}\mathbf{E}^H$, if we use an orthonormal basis for our encoding matrix **E**. Unfortunately, orthonormal bases are represented by square matrices of the same size as that of the parent matrix or the same size as **C** which is $N_s \times N_s$ in our case. Therefore, an orthonormal basis encoding matrix provides no cost advantage compared to standard shot-record imaging because we would have to perform N_s migrations, the same number as conventional shot-record migration (in fact doing so would be more costly than conventional imaging due to aperture considerations).

To circumvent the cost problem of using an orthonormal basis we truncate the columns of an orthonormal basis to form an encoding matrix that provides a substantial cost reduction, i.e. $N_e < N_s$. The missing columns contain features from the image that are lost in the reconstructed blended image. Therefore, we cannot reasonably expect to produce the same image as conventional shot-record migration at significantly reduced cost, but we may still be able to produce an image that appears "good enough" at reduced cost. Furthermore, crosstalk can be viewed as the result of discarding information from the image, where the crosstalk artifacts have a specific character based on how the shot-encoding discards information. This conclusion is similar to that obtained by Soubaras (2006) for the discrete Fourier basis but more general in application.

Cost comparison

To make a fair comparison of how various shot-encoding schemes perform with respect to one another, we must compare the quality of the images at the same computational effort. However, the number of migrations required is not a fair basis by which to compare computational effort because it neglects the impact of additional factors such as migration aperture, which is especially important when comparing against decimated shot-record migration. Therefore, we evaluate the computational effort of shot-encoding based on a measure that is a theoretical proxy for the total amount of floating point operations required per image. In this case, the total computational effort for migrating a dataset using shot-record migration is:

$$C_{SRM} = F N_s C_s, \tag{12}$$

where F is the number of floating point operations per shot-record, N_s is the number of shot-records, and C_s is the cost of migrating each shot-record. Similarly, the overall computational cost of migrating using blending is:

$$C_{BRM} = F N_e C_e, \tag{13}$$

where F is the number of floating point operations per blended shot-record (assumed to be the same as for regular SRM), N_e is the number of blended shot-records and C_e is the cost of migrating each one. In most cases, we expect the number of blended experiments, N_e, to be significantly less than N_s, which would indicate that the overall cost of imaging with blending is less than imaging with shot-record migration. However, the cost of imaging a single blended shot-gather is greater because of aperture considerations (i.e. $C_e > C_s$), so the overall advantage of blending is less clear. Of course, the actual computational cost will vary greatly based on computational architecture, and code efficiency.

For downward continuation, the cost of migrating a single shot-record is proportional to:

$$C_s = 2F N_x N_y N_z N_\omega = 2F L_s N_\omega. \tag{14}$$

In equation (14), N_x, N_y and N_z are the number of points in the migration volume for a single shot-record in their respective dimensions, N_ω is the number of frequencies, F is the number of floating point operations per point in space and frequency, and 2 represents the cost of extrapolating both the source and receiver wavefields. We combine $N_x N_y N_z$ into a single term L_S, which is the migration volume (or migration aperture) for a single shot-record. In the case of blended shot-record migration, the migration volume L_e is the number of distinct points

from the migration volume of each shot-gather in the blended shot-gather. For example, if the blended shot-record consists of shot-records that have independent migration volumes (i.e. the volumes do not overlap), then $L_e = N_s L_s$. Conversely, if the blended shot-gather is composed of shots that have almost identical migration volumes (i.e. the volumes overlap), then L_e is the number of distinct points in sum of the individual shot-record migration volume. In both cases, the total cost of migration is proportional to the number of experiments (shot-records) and the cost of migrating each experiment.

To determine whether blending offers a computational advantage over shot-record migration, we take the ratio of equation (12) and equation (13), substituting the appropriate values for C_s and C_e to produce,

$$\Gamma = \frac{2F L_S N_S N_\omega}{2F L_e N_e N_\omega} = \frac{L_S N_S}{L_e N_e} \tag{15}$$

where Γ is the cost ratio of shot-record migration to blended record migration. The value of Γ directly gives us a relative cost-ratio of shot-record migration to blended migration. For example, if Γ is greater than one, then blended imaging is more efficient than shot-record migration. Conversely, if Γ is less than one, then shot-record migration is more efficient than blended imaging. For practical purposes, a blended imaging scheme must at least be more efficient than break-even with SRM ($\Gamma \geq 1$) to be considered a success, while a good blending scheme would significantly reduce the cost of imaging by at least two-fold, $\Gamma > 2$. It is important to note that the overall computational cost reduction due to the reduced number of migrations by blending is countered by the increase in the migration volume L_e (Liu 1999; Romero *et al.* 2000; Zhang *et al.* 2005).

If the encoding matrix is frequency dependent, then the cost of blended imaging may depend on frequency if the number of encodings varies as a function of frequency. Thus, equation (13) becomes:

$$C_{BRM} = 2F L_e \sum_\omega N_e(\omega). \tag{16}$$

Again, taking the ratio of equation (16) and equation (12), we arrive at the following expression in the most general of terms for the ratio of the cost of blending and shot-record migration:

$$\Gamma = \frac{L_s N_s N_\omega}{L_e \sum_\omega N_e(\omega)}. \tag{17}$$

As with equation (15), when the value of Γ in equation (17) is less than 1, then SRM is less costly than blended imaging. If Γ is greater than 1, then SRM is more costly than blended imaging.

SHOT-ENCODING SCHEMES

In the following sections we demonstrate how the theory that we have developed can be used to construct new shot-encoding schemes and explain the characteristics of previous shot-encoding schemes as well. In particular, we discuss the following shot-encoding schemes: Hartley, modulated-shot migration, plane-wave migration, random time-delay and decimated shot-record migration. To begin, we design a new shot-encoding scheme that uses only amplitude weights. The advantage to amplitude encoding is that we do not have to use phase-shifts or time-delays, which may save computational cost depending on the type of migration used. One amplitude encoding that we have developed is the Hartley encoding although others are possible.

Hartley basis

A well-known orthonormal basis is the complex-valued discrete Fourier matrix (Strang 1997; Oppenheim 1999; Soubaras 2006). A real-valued alternative to the Fourier basis is the Hartley basis (Strang 1997; Tsitsas 2010). The Hartley encoding matrix is defined as,

$$\mathbf{E}_{m,n} = \cos\left(\frac{2\pi mn}{\wp}\right) + \sin\left(\frac{2\pi mn}{\wp}\right), \tag{18}$$

where m is the shot-index, n is the encoding index, and $\wp$ is the periodization index (Soubaras 2006). The relation to the Fourier transform is directly apparent, but the presence of the addition between the sine and cosine introduces additional cross-terms into the crosstalk matrix as follows,

$$\begin{aligned}\mathbf{C}_{k,l} = \sum_{n=0}^{N_e} &\cos(\psi_k)\cos(\psi_l) + \cos(\psi_k)\sin(\psi_l) \\ &+ \sin(\psi_k)\cos(\psi_l) + \sin(\psi_k)\sin(\psi_l),\end{aligned} \tag{19}$$

where $\psi_k = 2\pi kn/\wp$ and $\psi_l = 2\pi ln/\wp$. From equation (19) it is clear that there are additional off-diagonal components represented by the cross-terms between the $\cos(x)\sin(y)$ terms present in the expression. We note, that the cross-terms may be removed by using negative frequency values for the same encodings in equation (18) and then adding them to equation (18), because the sine function is odd (e.g. $\sin(-x) = -\sin(x)$). However, doing so would double the number of encodings required, from N_e to $2N_e$, or more importantly halve the number of encodings that we are able to use to capture unique information in the encoding matrix. Halving the

number of encodings with unique information is detrimental to the image quality because each unique encoding captures additional spatial information in the image (Stork 1999; Zhang *et al.* 2005; Soubaras 2006).

To understand why this is the case, we consider the relationship between sinusoids and spatial sampling theory. This relationship is derived directly from the encoding matrix by converting equation (18) from shot-indices to spatial coordinates. For example, if we let $m = x_m/\Delta x$ where Δx is the shot-sampling interval, and x_m is the actual shot-location in space, then equation (18) becomes:

$$\mathbf{E}_{m,n} = \cos(2\pi x_m n/(\Delta x \wp)) + \sin(2\pi x_m n/(\Delta x \wp)). \tag{20}$$

Using the relationship between the shot spatial wave-number, K, and the spatial sampling interval, $\Delta K = 1/\wp\Delta x$, then equation (20) is equivalent to:

$$\mathbf{E}_{m,n} = \cos(2\pi x_m n\Delta K) + \sin(2\pi x_m n\Delta K). \tag{21}$$

From equation (20) it is clear that when the encoding matrix is square (i.e. $N_e = N_s$) then the encoding matrix is unitary because the complete sum of sinusoids is unitary. Additionally, equation (21) shows that each additional encoding (specified by the n-index) increases the angular frequency of the argument to the sine and cosine functions. By using the relationship, $K = n\Delta K$, equation (21) shows that each additional encoding adds another spatial wave-number to the encoding matrix up to the maximum spatial wave-number as specified by the Nyquist sampling criterion (i.e. in the limit the encoding is equivalent to SRM). However, when we truncate the Hartley basis or truncate the encoding matrix, we restrict the maximum sampled wave-number, which means that the image is not fully sampled in the shot wave-number domain. Since we usually prefer to keep encodings corresponding to low wave-numbers, we construct an encoding matrix that is equivalent to an ideal low-pass spatial filter that uses the Hartley transform which creates the interesting banding patterns in the crosstalk matrix, Figures 3(a)–3(d).

Modulated-shot migration (Dispersive Fourier Transformation)

Modulated-shot migration, which we refer to as the DFT shot-encoding, is an encoding scheme that uses the discrete Fourier transform matrix as the encoding matrix (Soubaras 2006). Formally, the encoding matrix is given as:

$$\mathbf{E}_{m,n} = \begin{cases} \cos(Amn) - j\sin(Amn), & 0 \le n < N_e/2 \\ \cos(Amn) + j\sin(Amn), & N_e/2 \le n \le N_e \end{cases} \tag{22}$$

where m is the shot index, n is the encoding index, and A is $2\pi/\wp$ where $\wp$ is the previously discussed periodization distance, which is typically N_s for the unitary DFT encoding matrix. The crosstalk matrix for the DFT encoding is:

$$C_{k,l} = \sum_{n=1}^{N_e} \cos(Akn)\cos(Aln) + \sin(Akn)\sin(Aln). \tag{23}$$

Equation (23) is similar to equation (19) except without the cross-terms between sines and cosines. As with the Hartley encoding, we can consider the DFT encoding to operate in the wave-number domain as well by substituting the appropriate quantities, $m = x_m/\Delta x$, which leads to the same conclusion: DFT encoding acts as a low-pass spatial bandpass filter as shown by the banding in Figures 3(e)–3(h). The ringing in the crosstalk matrix is due to the lack of high wave-numbers from truncating the encoding matrix. However, modulated-shot migration differs significantly from Hartley encoding because DFT encoding requires both $+K$ and $-K$ values to properly illuminate the subsurface (Soubaras 2006).

Plane-wave migration

For plane-wave migration, the encoding matrix is defined by the maximum time-delay and the number of encodings. As mentioned in the literature, the maximum time-delay also determines the maximum wave-number in the blended image, and subsequently the crosstalk present in the final image (Tieman 1997; Duquet 1999; Liu 1999; Stork 1999; Zhang *et al.* 2005). To illustrate this consider the expression for the frequency-dependent encoding matrix for plane-wave migration which is given by:

$$\mathbf{E}_{m,n}(\omega) = \exp(-j\omega\tau_{m,n}), \tag{24}$$

where $\tau_{m,n}$ is the time-delay in seconds, at the m^{th} shot for the n^{th} plane-wave encoding. The time-delay, $\tau_{m,n}$, is related to the shot position and the blended experiment by the relation,

$$\tau_{m,n} = \frac{(t_{max} - 2nt_{max}/N_e)m}{N_s} - \frac{t_{max} - 2nt_{max}/N_e}{2}, \tag{25}$$

where n is the n^{th} encoding, m is the shot index, t_{max} is the maximum time-delay in seconds, and N_e is the number of blended experiments. Equation (25) requires $2t_{max}$ because plane-wave migration must create plane-waves with both positive and negative time-delays to ensure proper illumination throughout the image. As Stork (1999) and Zhang *et al.* (2005) note, the take-off angle of the plane-wave is related to the spatial wave-number in the image. The banding in the crosstalk matrix for plane-wave migration, Figures 3(i)–3(l), shows how

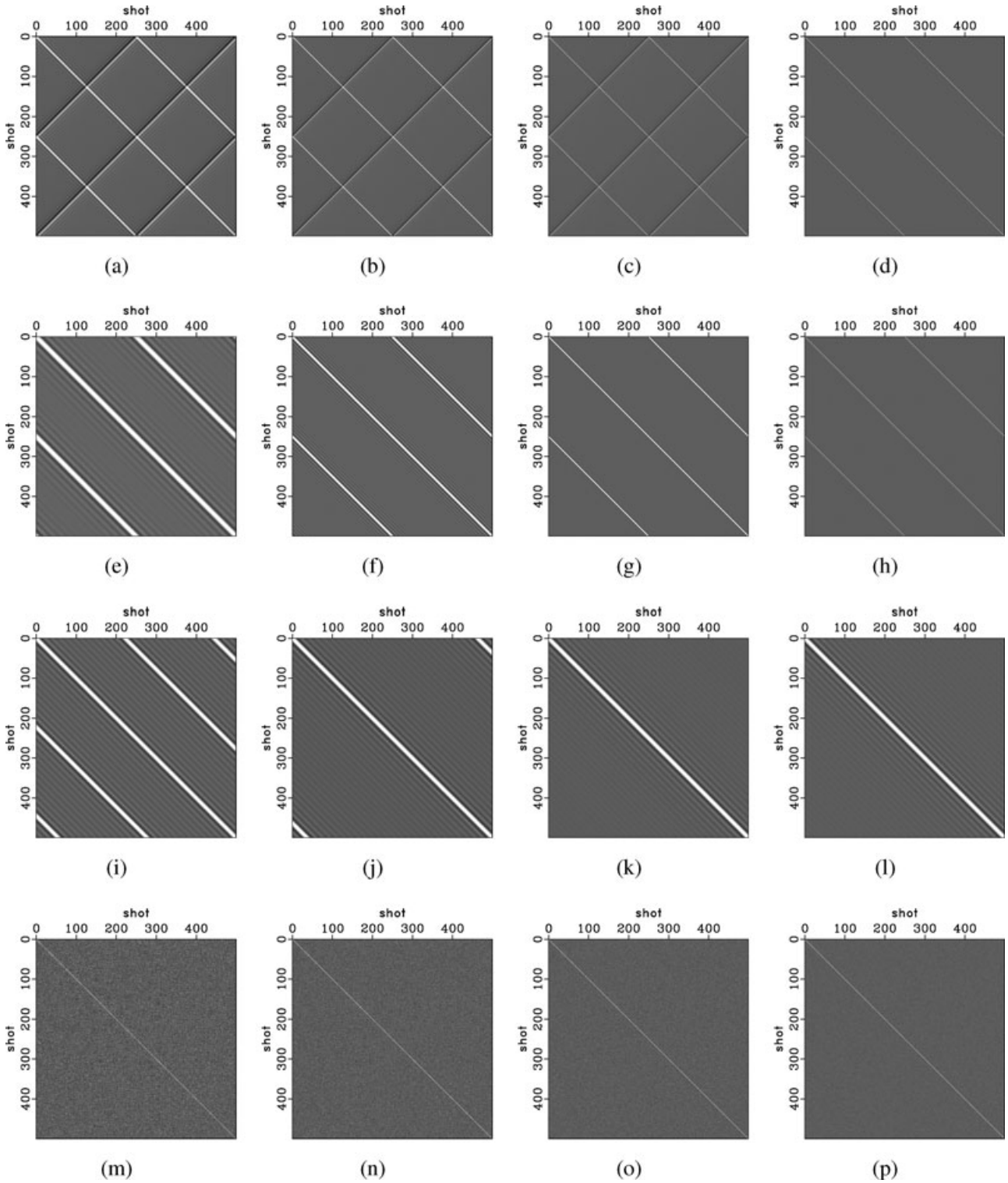

Figure 3 The real part of the crosstalk matrix for 3.0 Hz for the following shot-encoding schemes (top to bottom): Hartley, DFT, plane-wave and random-phase. Each column represents a different number of encodings used with the same shot-encoding scheme from (left to right): 25, 50, 100, 250. All of the crosstalk matrices except those for random-phase encoding have zero imaginary component, which we do not show here for brevity.

the take-off angle creates a low-pass spatial filter. In order to reconstruct the highest wave-numbers in the image, we must use plane-waves with greater and greater take-off angles (time-delays). This is a major shortcoming to plane-wave migration in the time-domain because additional time-delays substantially increase the computational cost of reverse-time migration.

In any case, the crosstalk matrix for plane-wave migration is given by:

$$\mathbf{C}_{k,l}(\omega) = \sum_{n=0}^{N_e} \exp(-j\omega[\tau_{k,n} - \tau_{l,n}]). \tag{26}$$

We expand equation (26) into:

$$\mathbf{C}_{k,l}(\omega) = \sum_{n=0}^{N_e} \cos(\omega[\tau_{k,n} - \tau_{l,n}]) + j\,\sin(\omega[\tau_{k,n} - \tau_{l,n}]). \tag{27}$$

We note that equation (27) is frequency dependent, meaning that a different crosstalk matrix exists for each frequency. In any case, when $k = l$ in equation (26), the complex-exponential is one, which produces the desired image. When $k \neq l$, then there is strong coherent crosstalk with a non-zero phase component (i.e. the sine term in equation (27) is non-zero). However, we note that when both positive and negative values of τ are swept, the sign of the phase-terms reverses, thereby removing them. Therefore, equation (27) is equivalent to the crosstalk matrices for both the Hartley and DFT encodings, equations (19) and (23) respectively, when the time-delays are sufficiently selected. However, the frequency-dependence of plane-wave migration is a significant difference between the encodings, which is why plane-wave migration and the other encodings do not produce the same result. As Stork (1999) shows, the time-delay for a given encoding can be converted to spatial wave-number. As with the DFT encoding, plane-wave migration requires two encodings for each spatial wave-number to properly illuminate the subsurface. It's important to note, that unlike the Hartley and DFT encodings, plane-wave migration evenly samples spatial wave-numbers up to a maximum wave-number that is determined by the maximum time-delay used.

Random time-delay

Random time-delay encoding delays the shots using delays specified by a uniform distribution Romero *et al.* (2000). The defining parameter for the uniform distribution is the maximum time-delay. Thus, the encoding matrix is given as:

$$\mathbf{E}_{m,n} = U(-t_{max}, t_{max}) \tag{28}$$

where U is a uniform probability distribution function with t_{max} the maximum time-delay for the shot-records. We can not formulate an analytic expression for the crosstalk matrix for random-time delay encoding. Instead, we can view the structure of the crosstalk matrix, Figures 3(m)–3(p), for one possible permutation of random time-delay encoding with the understanding that the crosstalk matrices for all similar encodings are more or less the same.

Decimated shot-record migration

As Stork (1999) and others have noted blended imaging is comparable to decimating our shot-records prior to imaging. Therefore, it is important to understand how different shot-encoding schemes compare against decimated shot-record migration (DSRM), because decimated shot-record migration has a few significant advantages over blended imaging:

- DSRM is easier to implement than shot-encoding because it does not require blending prior to imaging, and
- DSRM is less computationally expensive than blended imaging because each shot-record is migrated over a smaller migration aperture.

There is one major downside to DSRM though: we know that by decimating our data we introduce spatial aliasing for reflectors with high wave-numbers. For example, if we change our shot-sampling interval from Δx to $10\Delta x$ (i.e. decimate our data by a factor of 10), then the maximum wave-number of a reflector that we can avoid aliasing in our image is now 1/10 what it was before decimation due to the Nyquist criterion.

We note that it is also possible to consider DSRM as a shot-encoding scheme. To do so, we could construct an encoding matrix, whose columns consist of a single entry with all other rows being zero to select each individual shot-record for migration. Formally, the encoding matrix for DSRM is,

$$\mathbf{E}_{m,n} = \begin{cases} 1 & m = n\Delta s \\ 0 & \text{else,} \end{cases} \tag{29}$$

where Δs is the decimation factor (e.g. $\Delta s = 10$ to use every 10^{th} shot-record). The cross-talk matrix for decimated shot-record migration, is:

$$\mathbf{C}_{k,l} = \begin{cases} 1 & k = l = i\,\Delta s \\ 0 & \text{else.} \end{cases} \tag{30}$$

In equation (30), i represents integers in the range $[0,1,\ldots,N_s/\Delta s]$. The cross-talk matrix for DSRM is simply a decimated identity matrix.

RESULTS

We compare the Hartley, DFT, Plane-wave, and random-time shot-encoding schemes for the original Sigsbee2A dataset, which is comprised of 500 shot-records with a shot sampling interval $\Delta x_s = 45.72$m. For each shot-encoding scheme, we construct the encoding matrix as previously discussed. For Hartley and DFT encodings we use a periodization distance, $\wp = 250$, which is the optimal value for the Sigsbee dataset (based on migration aperture considerations). For plane-wave and random-time delay encoding we use a maximum time-delay of 9.0 seconds, which is the theoretical maximum given by Stork (1999). After constructing the encoding matrix, we generate the crosstalk matrices, Figure 3, for each encoding for a number of encodings: 25, 50, 100, and 250. Additionally, we compare the results of the encodings against the results obtained by using decimated shot-record migration using the same number of shot-records as encodings, i.e. the decimation factors are: 20, 10, 5, and 2 respectively. In this way, the number of migrations for blended imaging and decimated shot-record migration are identical.

We migrate the blended or decimated data using split-step downward continuation for frequencies sampled from 3−18Hz. Figures 4–5, show the stacked images for all of the encoding schemes (including decimated SRM) and the difference images computed by subtracting the normalized blended image from the normalized image from conventional shot-record migration, Figure 1(a). To make the comparison of difference images easier, we amplify (approximately 20 $\times$) and clip the difference images from all shot-encodings to the same scale. This ensures that changes in the difference images from encoding to encoding are directly comparable. Just by comparing the stacked images for the shot-encoding schemes we see that some shot-encodings are clearly superior to others. For example, plane-wave migration appears to produce a good quality image using a few number of encodings, whereas other shot-encodings need additional encodings to match the quality. As the difference images show, Figures 4–5, the crosstalk from the different shot-encoding schemes manifests itself very differently in the final stacked images. In all cases the amount and strength of the crosstalk decreases as the number of encodings used increases. For decimated shot-record migration, the difference image shows only the artifacts introduced by aliasing.

Additionally, we conduct a cost comparison of the various shot-encoding schemes using the previously outlined methodology, Table 1. For each encoding we provide best-case and worst-case speed-up, Γ, factors compared to shot-record migration using all 500 shot-records. The best case scenario is simply the ratio of the number of encodings compared to the number of individual shots. In the worst case scenario, we include the effect of migrating over a larger migration aperture. For the Sigsbee dataset, the blended migration aperture is approximately two-times the migration aperture of a single shot-record (i.e. $L_e = 2L_s$). In most cases, the actual speed-up relative to SRM is somewhere between these two values because the actual computational cost of imaging on modern computational hardware is strongly affected by hardware architecture and software optimization and so the increased cost due to the larger migration aperture may not be as bad as our worst-case scenario depicts. The cost advantage of shot-encoding compared to decimated SRM is less than optimal, with decimated SRM having a larger speed-up factor in almost every case.

We compare the F-K spectra of the: Hartley, DFT, plane-wave and DSRM shot-encoding schemes as Soubaras (2006) does, which illustrates how the various shot-encoding schemes sample the shot wave-number and frequency domain. In this case, we consider the effect that encoding has on on the image in terms of which spatial (shot) wave-numbers are reconstructed in the image relative to all of the wave-numbers obtained using conventional shot-record migration. Figures 6(a)–6(d) show the wave-numbers that these encodings select for 50 encodings.

Lastly, we compare the shot-encodings on an absolute basis by ranking them relative to one another using a measure of the energy in the difference images, or quality of the image, for each encoding. Formally, the measure of energy is simply the l_2-norm of the difference image. As the energy in the difference image is minimized, the quality of the stacked image is maximized. Thus, the best shot-encoding at a given cost minimizes the value of the energy. Figure 7 shows the comparison of the various shot-encodings as a function of the number of encodings used by comparing the overall energy in the difference image. Figure 7 shows that some shot-encoding schemes quickly approach zero in the difference image (i.e. the blended image is nearly identical to that obtained by conventional SRM), while others such as plane-wave migration have large differences regardless of the number of encodings used.

DISCUSSION

The unified theory of shot-encoding allows us to explain the results of previously developed shot-encoding schemes by using the crosstalk matrix to intuitively understand both the

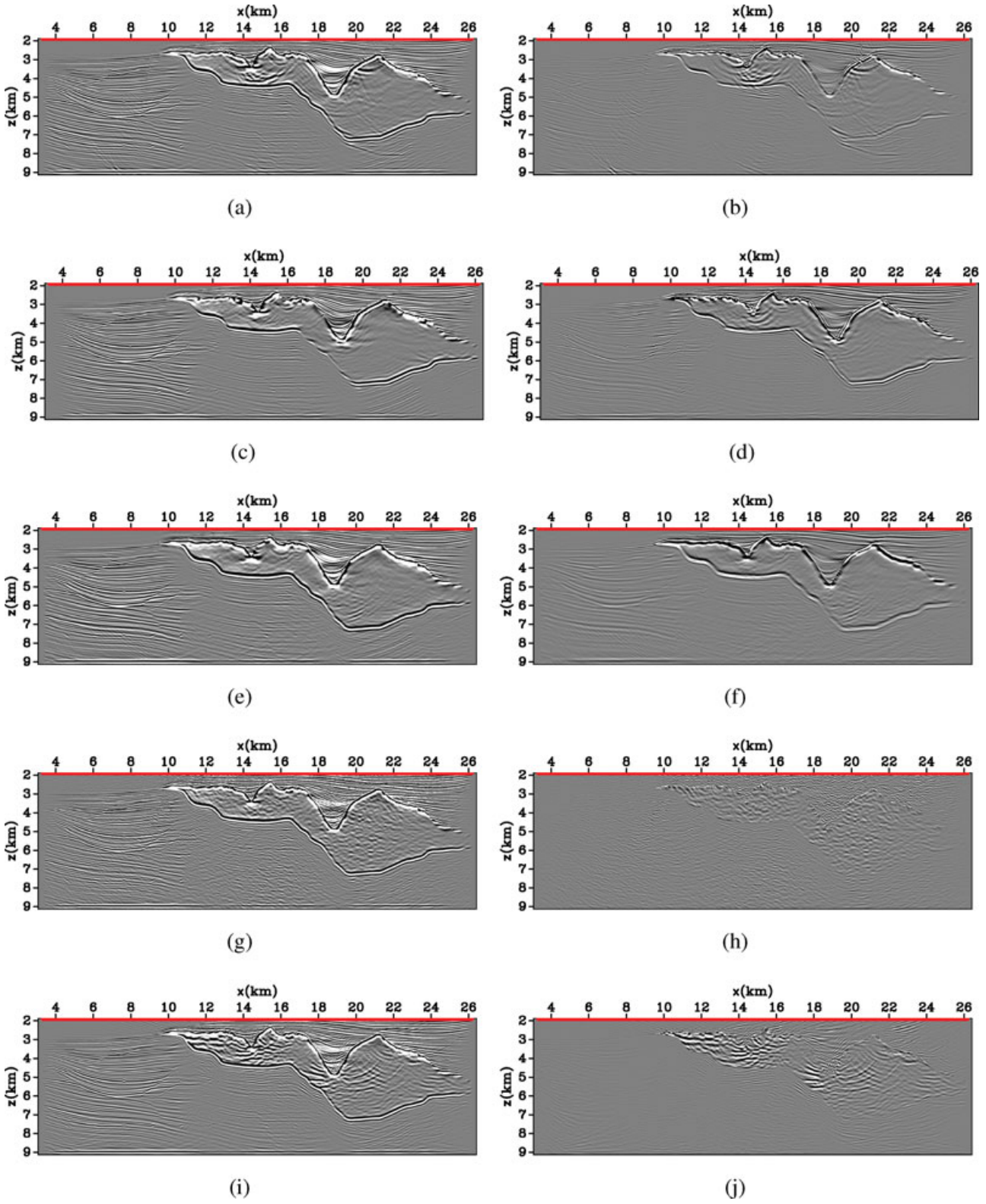

Figure 4 The stacked images (left) and difference images (right) for the following shot-encoding schemes (from top-bottom): Hartley, DFT (modulated-shot), plane-wave, random phase, and decimated shot-record migration. All encodings shown here use 50 encodings.

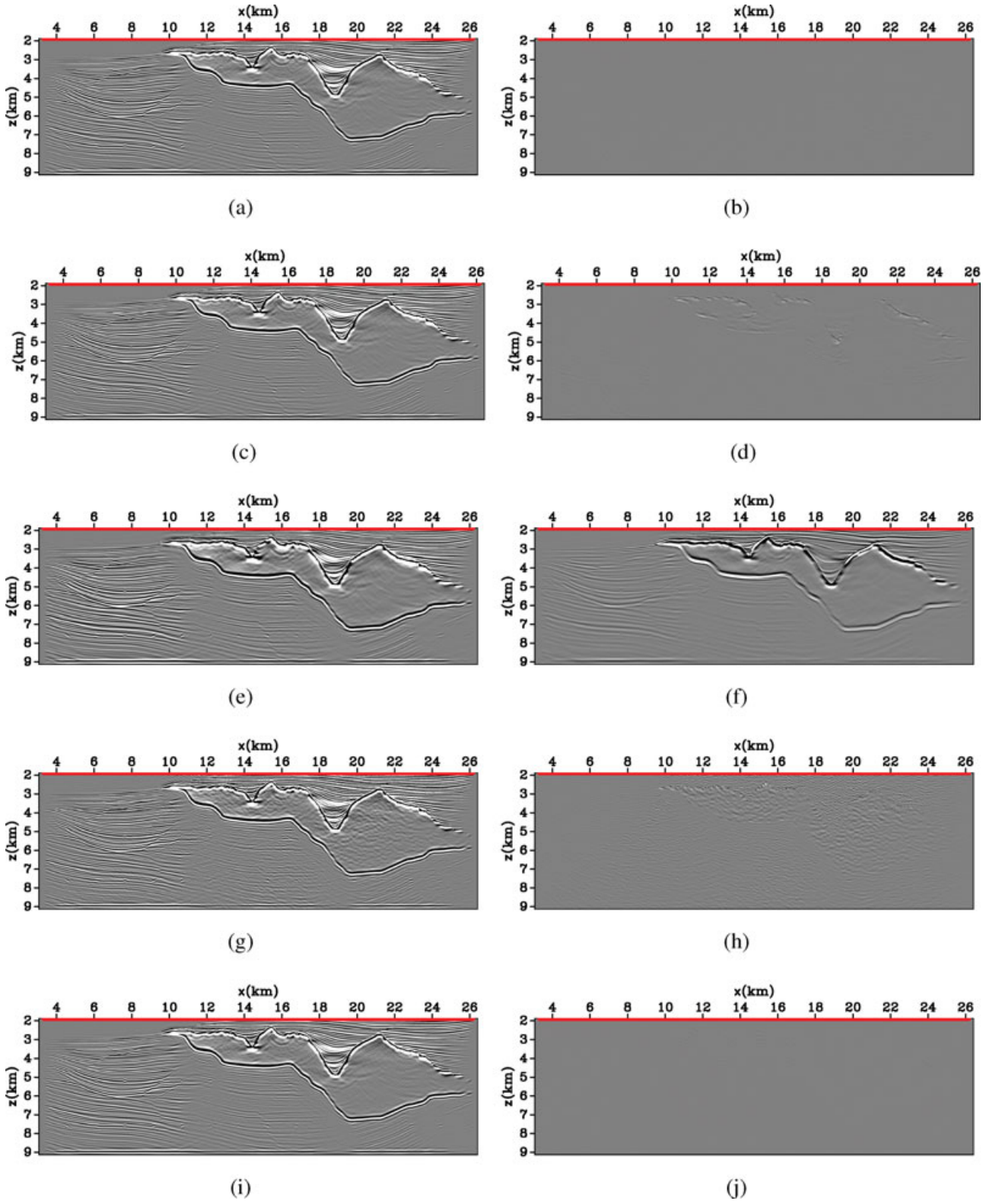

Figure 5 The stacked images (left) and difference images (right) for the following shot-encoding schemes (from top-bottom): Hartley, DFT (modulated-shot), plane-wave, random phase, and decimated shot-record migration. All encodings shown here use 250 encodings.

Table 1 Table comparing the computational cost of various shot-encoding schemes with the cost of conventional SRM for all 500 shot-records. The ratio Γ indicates the cost-advantage of blending over SRM. When Γ is greater than one, then blending is more efficient than SRM by that amount (e.g. $\Gamma = 2$ means the encoding is twice as efficient). We show Γ as a range from the worst-case scenario, migrating over a larger aperture significantly increases the computational cost, to the best-case scenario, where there is no increase in cost from migrating over a larger aperture.

Shot-encoding scheme	Hartley	DFT	Plane-wave	Random-time	DSRM
Frequency dependent	N	N	Y	Y	N
Migration aperture L_e	$2L_s$	$2L_s$	$2L_s$	$2L_s$	L_s
Γ - 25 experiments	10–20	10–20	10–20	10–20	20
Γ - 50 experiments	5–10	5–10	5–10	5–10	10
Γ - 100 experiments	2.5–5	2.5–5	2.5–5	2.5–5	5
Γ - 250 experiments	1–2	1–2	1–2	1–2	2

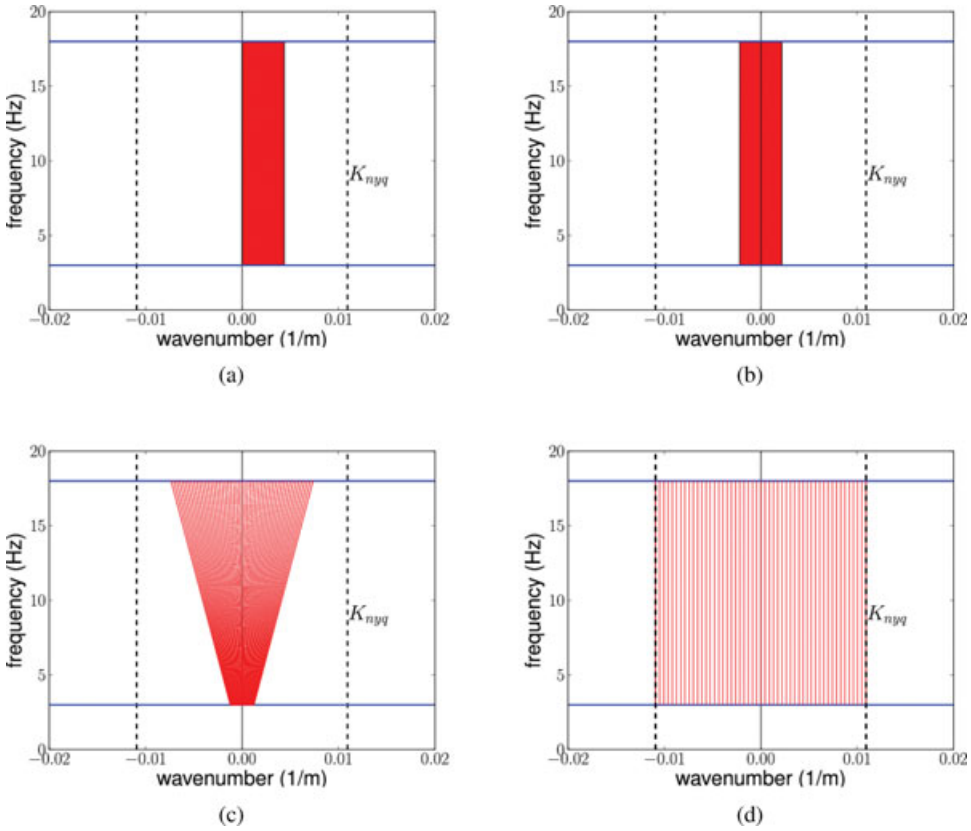

Figure 6 The F-K spectra for the (a) Hartley encoding, (b) DFT encoding, (c) Plane-wave migration, and (d) decimated SRM. All of the spectra show the result of using 50 encodings. The red (shaded) areas indicate the sampled wave-number frequency combinations for each shot-encoding scheme. Unshaded areas are not sampled. The horizontal blue-lines represent the minimum and maximum frequencies used in the migration, and K_{nyq} represents the Nyquist wave-number. For conventional shot-record migration the area between $-K_{nyq}$ and $+K_{nyq}$ (dashed lines) would be completely shaded, representing the selection of all wave-numbers for all frequencies.

strength and character of the crosstalk in the resultant images. As the crosstalk matrices, Figures 3(a)–3(p), for the various shot-encoding schemes show, the crosstalk matrix effectively predicts the overall quality of the final image without any need to produce a migrated image. However, the crosstalk matrix is somewhat limited because it cannot be used to predict the exact spatial distribution of crosstalk, as the spatial distribution depends on: the velocity model, the data, and

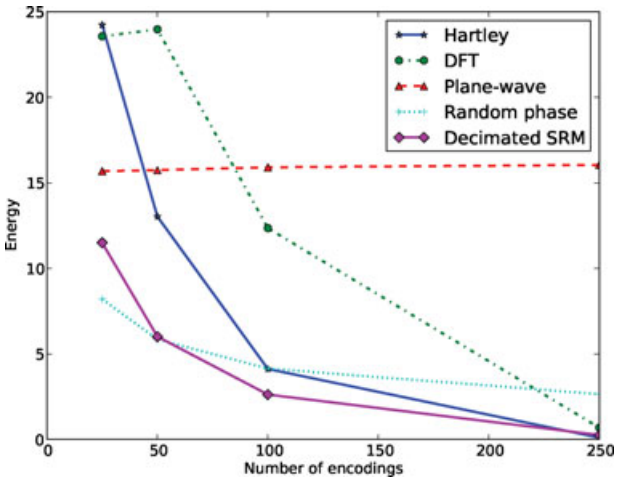

Figure 7 Plots of the energy (lower is better) in the difference image for the various shot-encoding schemes for a group of encodings. The different shot-encodings reconstruct the best quality image at different rates and with different efficiency.

the wavefield extrapolation engine used. If we could predict the spatial distribution of crosstalk with the crosstalk matrix, then we could potentially use that information to subtract out the crosstalk noise. We note that the crosstalk matrix for certain shot-encoding schemes, mostly plane-wave migration, have special physical meaning because the shots in the crosstalk matrix are ordered by their proximity in physical space. Thus, the crosstalk matrix for plane-wave migration indicates that the crosstalk forms as the sum of nearby shots (in physical space) with one another, which has significant practical implications as we discuss later. Additionally, we use the the theory of shot-encoding to develop a new class of shot-encoding schemes that rely solely on amplitude-weights. We only investigate one such encoding, the Hartley encoding, although many more are certainly possible. Amplitude encodings are potentially useful because they avoid the need to use long time-paddings for time-domain migration algorithms such as reverse-time migration, although we have not explicitly evaluated the suitability of shot-encodings for reverse-time migration.

After comparing the shot-encoding schemes against one another, we conclude that plane-wave migration appears to produce the best quality image at a given number of encodings Figures 4–5. Neither Hartley, DFT or random-time delay encoding produce images that are comparable to plane-wave migration. For all of the shot-encoding schemes, except plane-wave migration, the difference image energy decreases as the number of shot-encodings increase, Figure 5, which indicates that the crosstalk is being effectively suppressed as expected. Interestingly, decimated shot-record migration has the lowest difference energy relative to the shot-encoding schemes in all cases except for 25 encodings, in which case the resultant image is unusable for most purposes regardless of the shot-encoding scheme chosen although plane-wave migration seems to produce a better image at the same number of encodings (or migrations) used.

In the case of plane-wave migration the difference image remains fairly consistent as the number of encodings increases, Figure 7, which indicates that the difference image has an amplitude distortion relative to conventional shot-record migration. The amplitude distortion is consistent across the entire stacked image, but is not a scaling difference between the conventional SRM image and the plane-wave migrated image. Instead, the amplitude distortion is fundamentally related to the maximum take-off angle used for the plane-wave migration. To understand why this is the case, we need to examine the encoding matrix for plane-wave migration in the F-K domain, Figure 6(c). In the F-K domain, plane-wave migration evenly samples the F-K spectrum up to the maximum F-K combination allowed by the maximum take-off angle, which preferentially biases the F-K combinations present in the reconstructed image towards low frequency, low wave-number combinations which leads to spatial smearing of the reflectors. Thus the amplitude distortion present in the difference images, is really the spatial smearing of the reflectors, relative to the reflectors in the conventional SRM image. The crosstalk matrix for plane-wave migration explains this intuitively, Figure 3(l), as the crosstalk matrix shows that the crosstalk is equivalent to weighting and combining the nearby shots, which would logically result in spatial smoothing in the image. Even as we increase the number of encodings for plane-wave migration, we only introduce more samples in the range of F-K combinations allowed by the maximum take-off angle, which is effective at removing the non-smoothing crosstalk artifacts. However, if we want to reduce the spatial smoothing (i.e. the amplitude distortion), then we need to increase the maximum take-off angle in order to sample higher F-K combinations, which explains why Figure 7 has the same difference energy for plane-wave migration. As previously noted by Stork (1999), increasing the take-off angle permits crosstalk back into the image, which results in a tension between better amplitudes and the acceptable amount of crosstalk in the image. If we want less crosstalk and better amplitudes, then we fundamentally need to use more encodings with a larger maximum take-off angle. Theoretically, we would need to let the take-off angle tend towards 90 degrees (i.e. full coverage)

in order to correctly reproduce the amplitudes in the image (Liu 1999). It is important to note though that this conclusion depends on the F-K content of the data and the resultant image. If the image has only low wave-numbers (i.e. low dips) then smaller take-off angles should be sufficient to accurately capture the information in the image.

Similar arguments can be made based on the F-K spectra of the other shot-encoding schemes. In particular, the Hartley and DFT encodings, Figure 6(a)–6(b), show that they do not sample wave-numbers as a function of frequency, which means they under sample the high wave-numbers at high-frequencies, which leads to noticeable degradation of the image, or a "low frequency" quality to the image. As the number of encodings increases, and the Hartley and DFT encodings sample the higher wave-number/frequency combinations, the quality of the image significantly improves, and the difference energy decreases as expected. This is not a surprising result, as the conventional image of the Sigsbee2A dataset has large wave-numbers because of the presence of the salt body and steeply dipping faults. For decimated SRM, Figure 6(d), the decimation introduces aliasing artifacts into the image. As the decimation factor is reduced (i.e. we use more shots) the F-K spectra is sampled more adequately and the aliasing artifacts decrease in strength and coherency. Ultimately though, the aliasing and crosstalk artifacts both depend on both the model and the data because if the image only required small wave-numbers to be sampled, then we might find a reasonable image (free of crosstalk or aliasing artifacts) could be produced at a significantly reduced computational cost. On the other hand, if we need all the possible wave-numbers in the image (up to the Nyquist criterion), then we would expect that shot-encoding can not produce a reasonable quality image (versus conventional SRM) using fewer migrations than conventional shot-record migration because it is fundamentally a down sampling operation. Of course these considerations are frequency-dependent because low wave-numbers are adequately sampled at low frequencies , even at very coarse spatial sampling intervals, which would allow us to significantly decimate our data with no apparent degradation in the image.

Even though shot-encoding is a downsampling operation, it still produces reasonable results on most datasets because most datasets are somewhat oversampled. For the Sigsbee2A dataset, the decimated shot-record migrated images show that the dataset is oversampled in the shot-domain by approximately a factor of two because the decimated SRM image for 250 migrations, Figure 5(i), is almost identical image to the image from conventional shot-record migration. Thus, the best way to reduce the computational cost of imaging might be to simply decimate our datasets. Doing so has two significant downsides: 1-we throw away data that we paid to acquire in the field, and 2-the extra redundancy in the data is powerful for attenuating both incoherent and coherent noise in the resultant image. The same arguments apply to shot-encoding as well, because we are fundamentally downsampling (i.e. discarding data) by shot-encoding our wavefields. Subsequently, we expect that shot-encoding would produce degraded images when the noise is strong and/or when the dataset is not oversampled, which has been demonstrated by Stork (1999). Indeed, the only scenario under which shot-encoding could reasonable be expected to produce good quality images at a significant cost reduction are when the data are heavily oversampled and relatively free of noise, in other words on synthetic datasets.

Ultimately, the total computational effort required to produce an image with shot-encoding versus simple decimation determines whether or not shot-encoding is a worthwhile technology for reducing the computational cost of imaging. Table 1 shows that plane-wave migration and all of the shot-encodings for that matter have a significantly increased computational cost due to the need to migrate the blended dataset over a much larger aperture. Taking into account the effect of the increased aperture does not affect the comparison of the shot-encodings against one another, but it does affect the comparison between any of the shot encodings and decimated SRM, as we should effectively compare decimated SRM and shot-encoding at equivalent computational effort. In the worst case scenario for shot-encoding, this means that we should compare the shot-encoding results against those of decimated SRM using twice the number of shots. For example: the plane-wave migration result for 50 migrations should be compared against the result from decimated SRM using 100 shots. At equivalent computational effort, plane-wave migration does not appear to produce a significantly better image than decimated SRM which questions the justification for the use of plane-wave migration.

It is important to note though, that the same cost arguments apply to the other shot-encoding schemes presented here: namely that once one accounts for the increased cost due to the larger migration aperture used, the computational cost advantage of shot-encoding basically no longer exists given the image quality of decimated SRM. For three-dimensional (or large) surveys, the cost argument is even worse than for the Sigsbee example shown here because the migration aperture may be many times larger for a blended shot-gather than an individual shot-gather.

Lastly, it does not appear at that an "optimal" shot-encoding scheme exists, i.e. there is no shot-encoding scheme that will produce the same quality image as conventional SRM at reduced computational cost. As we have shown, shot-encoding is essentially a downsampling operation, which implies that all shot-encodings schemes introduce crosstalk into the image. If a shot-encoding scheme does not appear to degrade an image then the dataset is likely oversampled in the shot-domain and could likely be imaged using fewer shots at a lower overall computational effort. Moreover, as the industry trends towards higher frequency migrations both shot-encoding and decimated SRM will likely be less applicable in general, because the entire dataset will need to be used to prevent introducing significant artifacts at high-frequencies.

CONCLUSIONS

We compare the results of various shot-encoding schemes including: modulated-shot migration, plane-wave migration, random time-delay encoding and decimated shot record migration. Overall, we find that plane-wave migration performs the best out of the shot-encoding schemes that we have examined. However, we find that shot-encoding is fundamentally a down sampling operation and only appears to provide a significant cost reduction when the dataset is oversampled. When we take into account the increased computational cost of migrating blended datasets over larger apertures, the cost advantage of plane-wave migration (and shot-encoding in general) disappears; which leads us to conclude that decimated shot-record migration is more advantageous than shot-encoding in many situations. As we note though, there are some scenarios (e.g. full aperture synthetic data) in which shot-encoding may be advantageous to decimation.

ACKNOWLEDGEMENTS

We want to thank the sponsors of the Center for Wave Phenomena for financial support on this project. Also, we want to thank Dave Hale and Francesco Perrone for their insights on various aspects of this project. Lastly, we want to thank the contributors to the Madagascar software package.

REFERENCES

Akerberg P., Hampson G., Rickett J., Martin H. and Cole J. 2008. Simultaneous source separation by sparse radon transform. *SEG Technical Program Expanded Abstracts* **27**, 2801.

Beasley C.J. 2008. A new look at marine simultaneous sources. *The Leading Edge* **27**, 914.

Berkhout, A., Verschuur, D. and Blacquiere, G. 2009. Seismic imaging with incoherent wavefields. *SEG Technical Program Expanded Abstracts* 2894–2898.

Berkhout A.J.G., Blacquiere G. and Verschuur E. 2008. From simultaneous shooting to blended acquisition. *SEG Technical Program Expanded Abstracts* **27**, 2831.

Blacquiere, G., Berkhout, G. and Verschuur, E. 2009. Survey design for blended acquisition. *SEG Technical Program Expanded Abstracts* 56–60.

Duquet B. 1999. 3D plane wave migration of streamer data. *SEG Technical Program Expanded Abstracts* **20**, 1033.

Hampson G., Stefani J. and Herkenhoff F. 2008. Acquisition using simultaneous sources. *The Leading Edge* **27**, 918.

Howard M. 2007. Marine seismic surveys with enhanced azimuth coverage: Lessons in survey design and acquisition. *The Leading Edge* **26**, 480.

Huo, S., Luo, Y. and Kelamis, P. 2009. Simultaneous sources separation via multi-directional vector-median filter. *SEG Technical Program Expanded Abstracts* 31–35.

Kapoor S.J., O'Brian, M., Desta D., Atakishiyev I. and Tomida M. 2007. Subsalt imaging—the RAZ/WAZ experience. *SEG Technical Program Expanded Abstracts* **26**, 926.

Kim, Y., Gruzinov, I., Guo, M. and Sen, S. 2009. Source separation of simultaneous source OBC data. *SEG Technical Program Expanded Abstracts* 51–55.

Liu F. 1999. Plane wave source composition: An accurate phase encoding scheme for prestack migration. *SEG Technical Program Expanded Abstracts* **21**, 1156.

Liu F., Hanson D.W., Whitmore N.D., Day R.S. and Stolt R.H. 2006. Toward a unified analysis for source plane-wave migration. *Geophysics* **71**, S129.

Michell S., Shoshitaishvili E., Chergotis D., Sharp J. and Etgen J. 2006. Wide azimuth streamer imaging of mad dog; have we solved the subsalt imaging problem?. *SEG Technical Program Expanded Abstracts* **25**, 2905.

Moore I., Dragoset B., Ommundsen T., Wilson D., Ward C. and Eke D. 2008. Simultaneous source separation using dithered sources. *SEG Technical Program Expanded Abstracts* **27**, 2806.

Morton, S.A. 1999. Fastershot-record depth migrations using phase encoding. *SEG Technical Program Expanded Abstracts*, **17**, 1131.

Oppenheim, A. 1999. Discrete-time signal processing, 2nd edn. Prentice Hall.

Perrone, F. and Sava, P. 2009. Comparison of shot encoding functions for reverse-time migration. *SEG Technical Program Expanded Abstracts* 2980–2984.

Romero L.A., Ghiglia D.C., Ober C.C. and Morton S.A. 2000. Phase encoding of shot records in prestack migration. *Geophysics* **65**, 426.

Shan, G. and Biondi, B. 2008. Plane-wave migration in tilted coordinates. *Geophysics*, **73**, S185.

Shoshitaishvili, E., Lee, K., Michell, S. and Etgen, J. 2006. Fast wavefield migration for wide azimuth data. *SEG Technical Program Expanded Abstracts* 2524–2528.

Soubaras R. 2006. Modulated-shot migration. *SEG Technical Program Expanded Abstracts* **25**, 2430.

Spitz S., Hampson G. and Pica A. 2008. Simultaneous source separation: A prediction-subtraction approach. *SEG Technical Program Expanded Abstracts* **27**, 2811.

Stoffa, P.L., Sen, M.K., Seifoullaev, R.K., Pestana, R.C. and Fokkema, J.T. 2006, Plane-wave depth migration. *Geophysics* **71**, S261.

Stork C. 1999. How many p values do you want to migrate for delayed shot wave equation migration?. *SEG Technical Program Expanded Abstracts* **23**, 1041.

Strang, G. 1997. Wavelets and filter banks, rev. ed. Wellesley-Cambridge Press.

Sun, P. 1999. Prestack migration of areal shot records with phase encoding. *SEG Technical Program Expanded Abstracts*, **21**, 1172.

Temme P. 1984. A comparison of common-midpoint, single-shot, and plane-wave depth migration. *Geophysics* **49**, 1896.

Tieman, H.J. 1997. Improving plane-wave decomposition and migration, *Geophysics*, **62**, 195.

Ting, C. and Zhao, W. 2009. A simulated wide azimuth simultaneous shooting experiment. *SEG Technical Program Expanded Abstracts* 76–80.

Tsitsas, N.L. 2010. On block matrices associated with discrete trigonometric transforms and arising in wave propagation theory. *Journal of Computational Mathematics* **28**.

Womack J.E. 1990. Encoding techniques for multiple source point seismic data acquisition. *Geophysics* **55**, 1389.

Zhang Y., Sun J. and Gray S. 2007. Reverse-time migration: Amplitude and implementation issues. *SEG Technical Program Expanded Abstracts* **26**, 2145.

Zhang Y., Sun J., Notfors C., Gray S.H., Chernis L. and Young J. 2005. Delayed-shot 3D depth migration. *Geophysics* **70**, E21.